Valencia bridge fire tests: Validation of simplified and advanced numerical approaches to model bridge fire scenarios

J. Alos-Moya[1], I. Paya-Zaforteza[1*], A. Hospitaler[1], E. Loma-Ossorio[2]

[1]*ICITECH, Departamento de Ingeniería de la Construcción, Universitat Politècnica de València. Camino de Vera s/n, 46071 Valencia, Spain*

[2]*Fire Department of Valencia, Parque Central de Bomberos, Av de la Plata 20, 46013, Valencia, Spain*

Authors e-mail addresses: José Alos-Moya: joalmo11@upv.es
Ignacio Paya-Zaforteza: igpaza@upv.es
Antonio Hospitaler: ahospitaler@upv.es
Eduardo Loma-Ossorio: eloma-ossorio@valencia.es

Abstract

Bridge fires are a major concern and the subject of many studies that use numerical models. However, experimental studies are still required to test the validity of these numerical models and improve their accuracy. This paper uses temperature results of the Valencia bridge fire tests carried out at the Universitat Politècnica de València, in Valencia (Spain) to calibrate the fire models that constitute the first step in modeling any bridge fire event. The calibration is carried out by both a simplified approach (Heskestad & Hamada's correlation) and advanced numerical models (Computational Fluid Dynamics models built with the Fire Dynamics Simulator –FDS- software).

The Valencia bridge fire tests involved four fire scenarios under a composite bridge with Heat Release Rate (HRR) values between 361 and 1352 kW. The results show that applying Heskestad & Hamada's correlation gave good results when used within its limits (HRR<0.764 MW) but did not work well beyond them, which means it would be suitable for planning reduced scale bridge fire tests but not in the analysis of real bridge fires. On the other hand, FDS provides good predictions of the temperatures and can be used to study bridge fire responses. This work is therefore an important step forward in the study of bridge fires and towards the improvement of the resilience of infrastructure networks vis-à-vis fire hazards. It also highlights the problems that can arise in fire tests in the open air, the influence of the wind being of critical importance.

Keywords: numerical modelling, Valencia bridge fire test, composite (steel-concrete) bridge, mass loss rate, bridge fire, bridge resilience.

* Corresponding author. Tel: +34 963875623; fax: +34 963877568

Notation

A_{fire} = Footprint of the fire (m^2)

b = Effective plume radius at the intersection with the ceiling elevation (m)

c_p = specific heat of the air = 1.005 ($kJ \cdot kg^{-1} \cdot K^{-1}$)

D = Fire equivalent diameter (m)

E_i = Temperature in a particular thermocouple in an experimental test (ºC)

g = Gravitational acceleration = 9.81 (m/s^2)

H = Ceiling height above the burning fuel (m)

L_f = Flame length (m)

L_f / H = ratio used to difference between strong and weak plume.

$\dot{m}$ = Mass loss rate (kg/min)

$\dot{m}''$ = Mass loss rate per unit area ($kg/m^2/s$)

M_i = Temperature in a particular thermocouple in the model (ºC)

Ma = Mach number

Q = Heat Release Rate (kW)

Q_c = Convective Heat Release Rate (kW)

r = Radial distance from axis of the fire plume (m)

s = side of the square pan (m)

T = Temperature at a particular point (ºC)

T_p = Temperature at a particular height in the centerline of the plume (ºC)

T_∞ = Ambient temperature = 20 (ºC)

z_b = Vertical coordinate of the fuel top surface inside the pan (m)

ΔH_c= Net heat of combustion (MJ/kg)

ΔT = Excess gas temperature at a point at a particular distance from the centerline of the plume. It is equal to $T - T_\infty$ (ºC), T being the temperature at the point considered and T_∞ the ambient temperature.

ΔT_p= Excess gas temperature in plume at the ceiling level. It is equal to $T_p - T_\infty$ (ºC), T_p being the temperature on the centerline at the impingement point on the ceiling.

Δ = bias factor of the model.

ε_m = material emissivity

θ = True value of the temperature (ºC)

λ = conductivity (W/mºC)

ρ = density (kg/m^3)

ρ_∞ = Gas density at ambient temperature = 1.204 (kg/m^3)

σ_E= Experimental standard deviation (due to measurements)

σ_M= Model standard deviation (due solely to the model)

χ_r = radiative fraction.

ω_0= Relative uncertainty of the measured output quantity

ω_E = Experimental relative standard deviation, σ_E / θ

ω_M = Model relative standard deviation, σ_M / [$\theta \cdot(1+\delta)$]

ω_i = Relative uncertainty of the devices that measure the various input parameters that the model requires.

1. Introduction

The harmful consequences of bridge fires (see e.g. Peris-Sayol et al.[1]) have given rise to significant research in recent years (see a summary e.g. in Garlock et al. [2] and Quiel et al.[3]). This research is based on the use of numerical models to analyze previous fire incidents (see e.g. Alos-Moya et al. [4], Gong & Agrawal [5], Godart et al. [6]) as well as the study of bridge responses to hypothetical fire scenarios (e.g. Peris-Sayol et al. [7] and Nahid et al. [8]).

The numerical analysis of bridge fires involves: (1) fire models to obtain the gas temperatures surrounding the structure, (2) heat transfer models to obtain the temperatures on the surface and within the bridge elements and (3) structural models to obtain the bridge's mechanical response. The first step is therefore to model the fire itself, and this has been done by different approaches; some researchers have built complex fire models using Computational Fluid Dynamics (CFD henceforth) (see e.g. Alos-Moya et al. [4], Peris-Sayol et al. [9], Gong and Agrawal [5]), while others have proposed simplified approaches based on the use of fire curves (see e.g. Payá-Zaforteza & Garlock [10]) or radiation heat fluxes (Quiel et al. [3]). Modeling a fire event is always challenging, since numerical models and simplified curves have been widely applied and validated by fires in buildings and tunnels (see e.g. Buchanan [11], Albero et al [12], Quiel et al. [13], Rackauskaite et al. [14], Maraveas and Vrakas [15], Ji et al. [16]), but, as pointed out by Payá-Zaforteza & Garlock [10], bridge fires have specific features and deserve a particular approach. To obtain an accurate bridges fire response, the numerical and simplified approaches need to be validated by experiments. However, the dimensions of bridge structural elements, the magnitude of the fire loads in bridge fires and the difficulties of carrying out open-air fire tests make experimental work on bridge fires rather complex and expensive. As a result, this type of work, e.g. the Valencia bridge fire tests carried out by Alos-Moya et al. [17], is not often undertaken. These tests consisted of reproducing different fire scenarios under a composite I-girder bridge built at the Universitat Politècnica de València, in Valencia, Spain. These conditions (fire positions and bridge deck structural system) were chosen because a previous statistical analysis of bridge fire incidents carried out by Peris-Sayol et al. [1] showed that (a) composite I-girder bridges are especially vulnerable to bridge fires and (b) the worst possible position for the fire is under the bridge deck.

Within this general context, the objective of the present study is to calibrate the numerical and simplified approaches available to model this type of fire. The Valencia bridge fire tests (Alos-Moya et al. [17]) are used to analyze the accuracy of two approaches (jet ceilings and Computational Fluid Dynamics) in reproducing the temperatures in the gases around the

bridge during the experiments. This analysis enables both the calibration of the models used and establishes their application limits. The authors consider that the results obtained are a crucial step towards the development of a performance-based approach that can be used to improve the resilience of bridge systems against fire hazards.

The paper is structured as follows: Sections 2 and 3 describe the experimental bridge and summarize the features of the fire tests used to validate fire models. The validity is studied of both the simplified (jet ceilings, Section 4) and advanced calculation methods (CFDs, Section 5) used to predict the results of the fire tests. Section 6 describes an uncertainty analysis of the results obtained by advanced calculation methods, and Section 7 summarizes the main conclusions of the research carried out and points to areas in which future work is required.

2. Case study and methodology

The reduced-scale bridge used in the present study was a simply-supported bridge specifically designed by the authors in order to carry out the tests detailed in Alos et al. [17]. The bridge had a span of 6.0 m and a vertical clearance of 1.9 m. The structure consisted of two IPE-160 steel girders which supported a 0.15 m thick reinforced concrete slab connected to the steel girders through 62 shear studs. The S355-JR steel employed for the girders showed yield stresses of between 344 and 377 MPa. The concrete slab compressive strength was 33 MPa. Bridge elevation, abutment details and deck details are shown in Fig. 1. Further information on the geometry and the materials used can be found in Alos et al. [17].Two auxiliary steel frames were placed over the deck to sustain the LVDT’s that monitored the deck deflections during the fire tests.

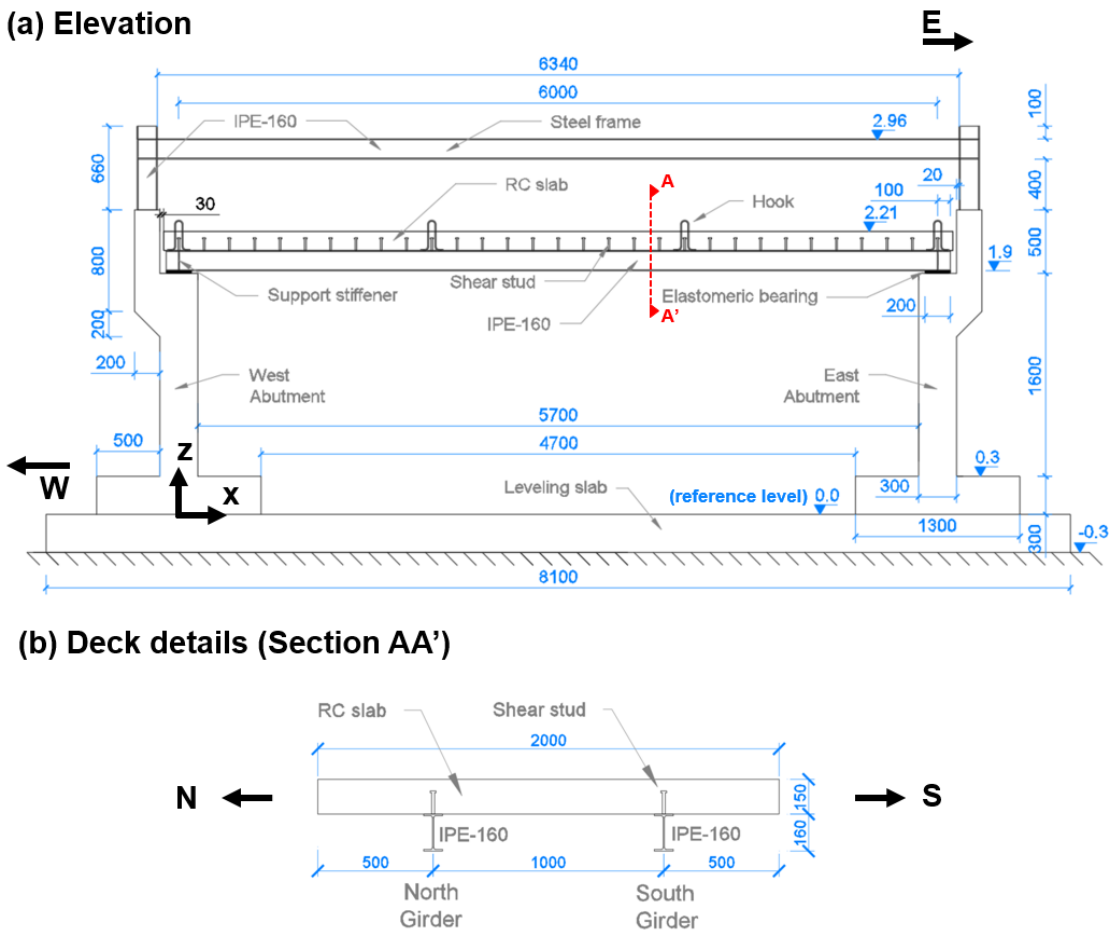

Figure 1. Experimental bridge: (a) elevation, (b) deck details. All the dimensions are expressed in mm. All the levels (z coordinates) are expressed in m.

3. Experimental approach

3.1. Fire scenarios

The Valencia fire tests involved eight fire tests with four different fire scenarios. The fire loads were located under the bridge and consisted of different quantities of gasoline poured into steel pans of different dimensions. The present study calibrates the fire models using results from four tests (tests 2, 4, 7 and 8) out of the eight tests carried out. These four tests were chosen because they best characterized the scenarios studied. Tests 1 and 3 were discarded for 2 and 4 due to the smaller influence of the wind in the latter. Tests 5 and 6 were discarded for 7, since the latter was the only one without a protected zone over the fire load. Table 1 gives details of the position and magnitude of the fire loads during the tests. The volume of gasoline used was obtained by weight and assuming a density of 740 kg/m^3 [18]. Four views of the tests are shown in Fig. 2.

It must be noted that the experimental bridge was not a replica or a reduced scale model of a specific bridge. The experimental bridge was designed to reproduce a structural system very common in highway bridges and the fire scenarios were defined to enable the study of some important aspects that previous studies [1,4, 7, 9, 19] on bridge fires had highlighted, such as: (1) the impingement of the flames on the bridge deck, (2) the spread of flames, heat and smoke between two adjacent bridge girders, (3) the creation of significant longitudinal thermal gradients along the bridge girders and (4) the influence of the fire load position on gas and bridge temperatures.

Fire Scenario	Test	Fire Location	HRR (kW)	Gasoline			Side	Pan Location	
				Weight (kg)	Volume (l)	Thickness (cm)	s (m)	x (m)	z (m)
Fire 1	Test 2	mid-span	426	17.5	23.6	9.5	0.5	3	0.2
Fire 2	Test 4	mid-span	1130	0.7	50.9	9.1	0.75	3	0.2
Fire 3	Test 7	abutment	361	18.1	24.5	9.8	0.5	5.59	0.5
Fire 4	Test 8	mid-span	1352	41.6	56.2	10	0.75	3	0.8

Table 1. Fire scenarios employed in the validation

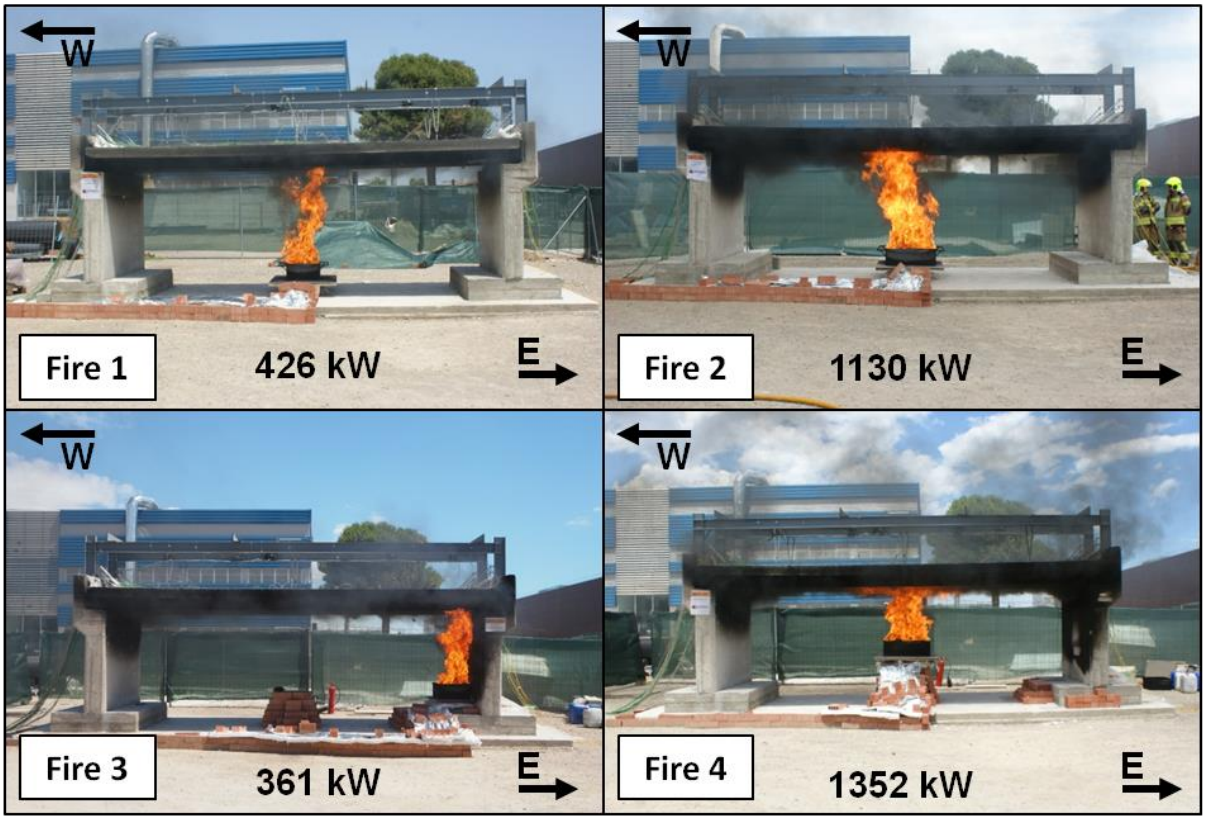

Figure 2. Views of the fire scenarios considered. Images include the power (Heat Release Rate) of the fire in each test.

3.2. Mass loss rate

Fig. 3 gives the mass loss rate recorded during the four validation tests. This value is important as when it is value is multiplied by the gasoline net heat of combustion (Δh_c) (43.7 MJ/kg) [18] the Heat Release Rate (HRR) of the fire is obtained. The HRR is a key variable in characterizing fires in the models used in fire engineering.

In Fig. 3 the growth zones in each of the tests can be distinguished. The plateau is only clearly defined in Fires 1 and 3, in which the fire load is lower. In the stronger fires the higher dispersion of the average values shown in Table 1 can be seen, which was calculated excluding the growth and decay phases. While in Fire 2 the higher mass loss values can be attributed to gusts of wind, the steady growth during Fire 4 is associated with the higher radiation from the bridge deck due to the lower distance between deck and pan filled with gasoline. This radiation is progressively increased during Fire 4 due higher deflections recorded during the test [17].

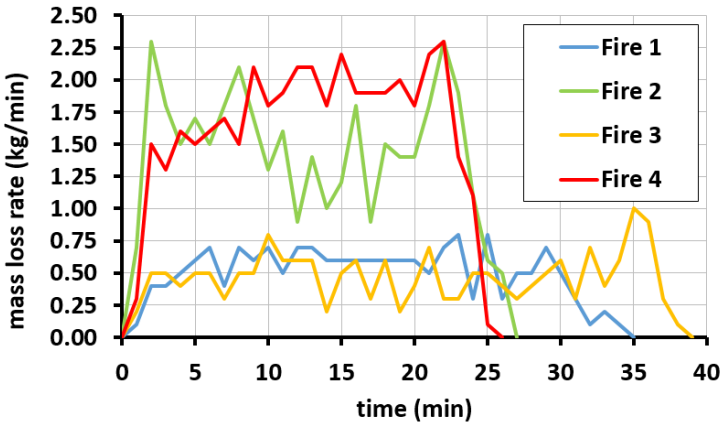

Figure 3. Mass loss rate evolution during the tests

3.3. Gas temperatures

Gas temperatures were measured by 23 1.5 mm Type K thermocouples (TCs) with stainless steel sheaths arranged in six horizontal thermocouple trees (TCTs) and one vertical TCTs. Fig. 4 shows the thermocouple layout. Every horizontal TCT had 3 TCs and the vertical TCT had five TCs. Regarding the nomenclature of the TCs in the horizontal TCTs: "G" indicates GAS, "S", "C" and "N" mean South Region, Central Region and North Region, respectively (see Fig. 4), and the number at the end indicates the section in which the TC is placed. The vertical TCT was used to measure temperatures in the plume. Regarding the nomenclature of the TCs in the vertical TCT: "V" indicates that the TC belongs to the vertical thermocouple tree and the number at the end indicates the order, starting from the TC closest to the pan.

Table 2 includes the average values of the gas temperatures in the four zones (North, South and Central regions and Fire plume) into which the space surrounding the bridge was divided. It also shows the maximum values in two of these regions (Central and Fire Plume), which are used in Section 6.3.

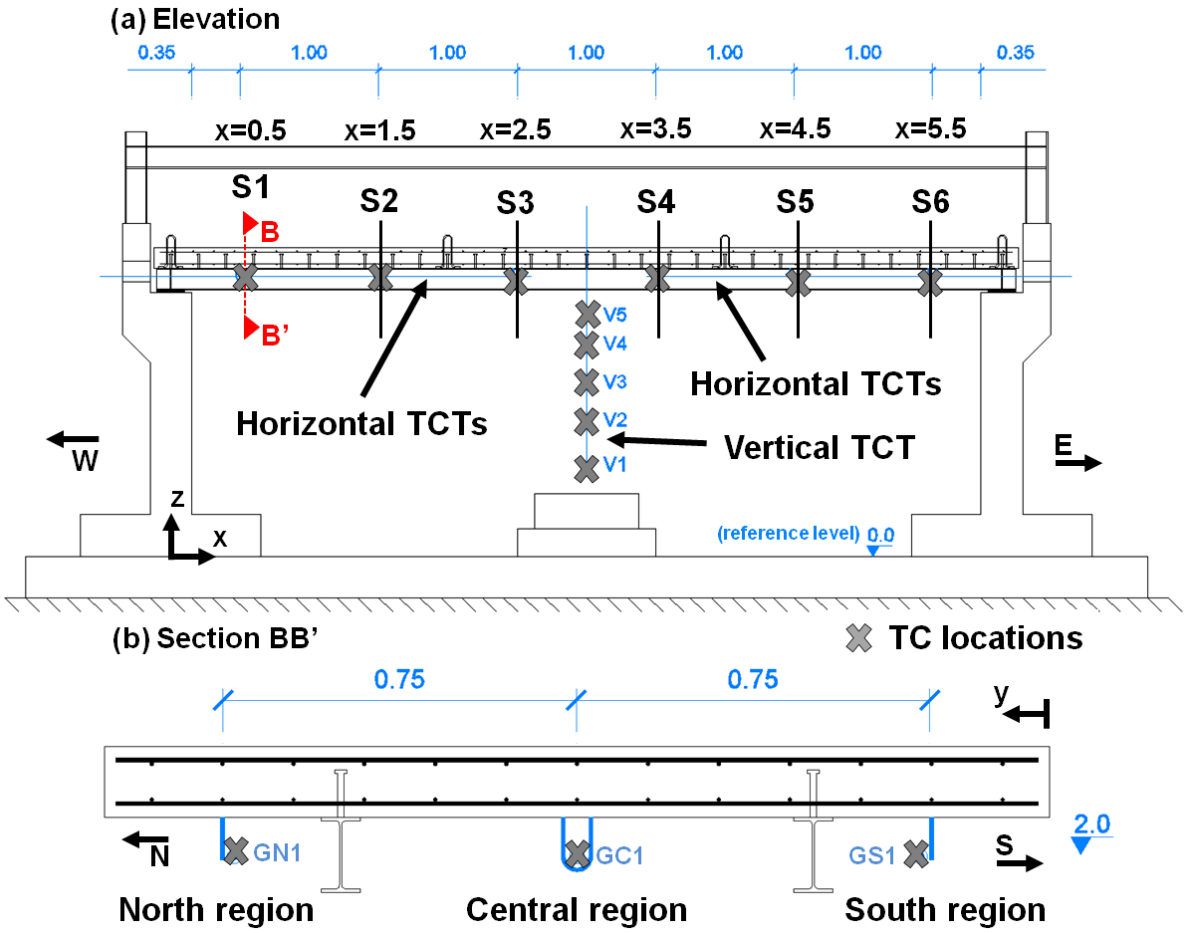

Figure 4. Gas thermocouple distribution. All dimensions are given in m.

Table 3 includes the time intervals selected to obtain the average values. As can be seen in Fig. 3, these values ensure that the averages were obtained in the plateau zones. It should be remembered that the thermocouple response to temperature changes in gas is almost instantaneous.

	x (m)	South region	North region	Central region		z (m)	Fire plume	
		Aver. T (ºC)	Aver. T (ºC)	Aver. T (ºC)	Max. T (ºC)		Aver. T (ºC)	Max. T (ºC)
Fire 1	0.5	89	101	112	172	1.73	206	402
	1.5	111	135	141	218	1.54	171	387
	2.5	154	185	221	398	1.24	236	549
	3.5	122	176	200	314	0.99	335	688
	4.5	87	108	122	183	0.65	542	827
	5.5	81	81	103	150	-	-	-
	x (m)	South region	North region	Central region		z (m)	Fire plume	
		Aver. T (ºC)	Aver. T (ºC)	Aver. T (ºC)	Max. T (ºC)		Aver. T (ºC)	Max. T (ºC)
Fire 2	0.5	206	176	222	318	1.73	450	774
	1.5	293	230	298	451	1.54	381	749
	2.5	446	310	463	711	1.24	405	853
	3.5	397	274	411	760	0.99	501	896
	4.5	207	187	247	525	0.65	685	883
	5.5	174	141	199	365	-	-	-
	x (m)	South region	North region	Central region		z (m)	Fire plume	
		Aver. T (ºC)	Aver. T (ºC)	Aver. T (ºC)	Max. T (ºC)		Aver. T (ºC)	Max. T (ºC)
Fire 3	0.5	54	63	76	141	1.95	422	614
	1.5	63	67	94	158	1.69	387	564
	2.5	83	31	122	190	1.41	462	748
	3.5	112	109	162	234	1.13	515	698
	4.5	158	153	229	306	0.85	739	866
	5.5	315	276	403	568	-	-	-
	x (m)	South region	North region	Central region		z (m)	Fire plume	
		Aver. T (ºC)	Aver. T (ºC)	Aver. T (ºC)	Max. T (ºC)		Aver. T (ºC)	Max. T (ºC)
Fire 4	0.5	217	232	295	440	1.89	701	949
	1.5	346	362	465	644	1.73	672	905
	2.5	559	41	713	955	1.54	766	938
	3.5	558	511	712	968	1.44	726	896
	4.5	276	289	427	647	1.25	646	909
	5.5	241	231	332	537	-	-	-

Table 2. Average temperatures (Ave. T (ºC)) and maximum temperatures (Max. T (ºC)) recorded during the tests. Average values were calculating during the intervals defined in Table 3.

Fire Scenario	Initial time (s)	Last time (s)	Total time (s)
Fire 1	400	1200	800
Fire 2	200	1300	1100
Fire 3	200	2000	1800
Fire 4	700	1300	600

Table 3. Intervals considered to obtain average temperatures

Further information on the gas temperatures recorded can be found in [17].

4. Simplified approach to modeling the Valencia bridge fire tests. Heskestad & Hamada's correlation.

A large number of models are used in the field of fire engineering, including (from low to high complexity): 1) nominal curves, 2) equivalent exposure time, 3) parametric fires, 4) localized fires, 5) zone models, and 6) CFD models. At the present time there are no nominal curves, equivalent exposure time or parametric fire models available specifically for bridge fires, although certain authors (Peris-Sayol et al. [19], Quiel et al. [20]) have analyzed the factors that play a role in the maximum temperatures reached in the bridge and its surroundings during a blaze. The first simplified models that could be used to study bridge fires were thus the *localized fire* and the more specialized *ceiling jet* models. Their potential for application to bridge fires is analyzed below.

4.1. Ceiling jets

4.1.1. Theoretical background

According to Alpert [21], a ceiling jet refers to "the relatively rapid gas flow in a shallow layer beneath the ceiling surface that is driven by the buoyancy of the hot combustion products from the plume". The ceiling jet flow emerges from the region of plume impingement on the ceiling, moving radially away from the fire. As it does so, the layer grows thicker by entraining room air, which cools the gases in the jet and reduces its velocity. Similarly, the ceiling also cools down the portion of the jet adjacent to it. Fig. 5 shows a sketch of the ceiling jet concept and a photograph of one of the tests on the experimental bridge carried out at the Universitat Politècnica de València.

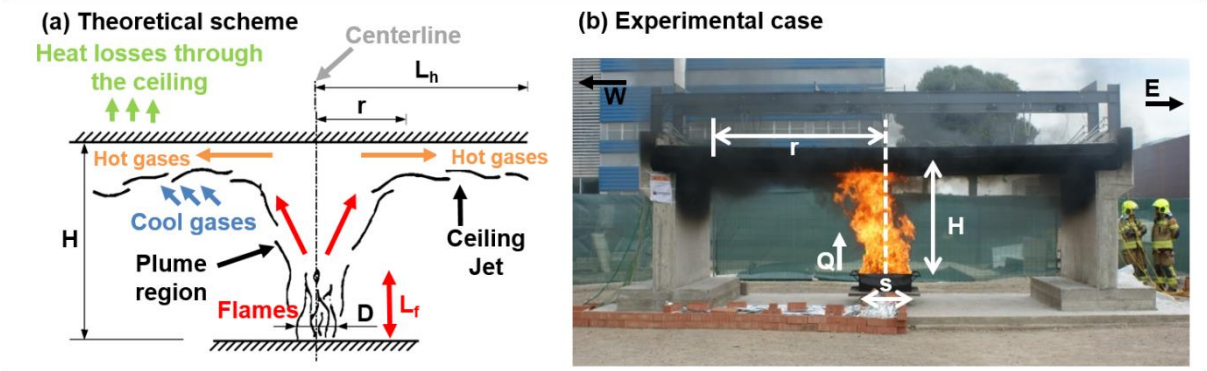

Figure 5. Ceiling jets with flame impingement: (a) Theoretical scheme, (b) Experimental case. Fig. 7a adapted from Eurocode 1 Part 1-2.

Depending on the L_f/H ratio (see Fig. 5b), where L_f is the flame length and H is the vertical distance between the burning fuel and the ceiling, a distinction is made between weak plumes (where convection is the dominant mode of heat transfer) and strong plumes (where

thermal radiation will be equally or more important than convection) [22]. There is no clear boundary between both types of plume, but Alpert's general theory for weak plumes [21, 23] was explicitly obtained for cases in which the flame height is much smaller than the distance between the burning fuel and the ceiling, while Heskestad & Hamada's theory [24] for strong plumes was validated for L_f/H ratios ranging from 0.2 to 2.0. In the present study, the flame length L_f was obtained using Heskestad's equation Eq. 1 [25].

(1) $$L_f = -1.02 \cdot D + 0.235 \cdot Q^{2/5}$$

Where:

Q = Heat Release Rate (kW)

D = Equivalent diameter (m) obtained assuming that the fire source is a circle with the same area as that of the real fire source. For square pans, D is given by Eq. 2:

(2) $$D = 2 \cdot s / \sqrt{\pi}$$

where s is the side of the square pan.

Table 4 shows the application of Eqs. 1 and 2 to the Valencia bridge fire tests analyzed in this paper to obtain the flame length and resulting L_f/H ratio. They show that the fire is clearly impinging on the concrete slab ($L_f/H > 1$) in the four scenarios, so that the four tests are therefore in the strong plume field. This shows that Hamada and Heskestad's correlation [24] is the best simplified approach to estimating gas temperatures. It should be noted that Kowslowski & Motevalli's correlation [26], obtained specifically for channel configurations (i.e. fires confined between two longitudinal elements) for 5.2 kW fires, cannot be applied to the Valencia bridge tests because it is only applicable to weak plumes with much lower HRRs.

Fire Scenario	Pan side, s (m)	Diameter, D (m)	HRR (kW)	Flame length, L_f (m)	Height, H (m)	L_f/H (m)
Fire1	0.5	0.56	426	2.07	1.85	1.12
Fire2	0.75	0.85	1130	3.05	1.85	1.65
Fire3	0.5	0.56	361	1.9	1.55	1.23
Fire4	0.75	0.85	1352	3.34	1.25	2.67

Table 4. L_f/H ratios from Eq. 1 for the fire scenarios analyzed.

4.2. Heskestad & Hamada's correlation

Heskestad & Hamada [24] measured ceiling jet temperatures for L_f/H ratios ranging from 0.3 to 3.0 for propane burner fires ranging from 12 to 764 kW beneath unconfined ceilings with H up to 2.5 m. Their results were employed to obtain the increment of the gas temperature below the ceiling from the increments of temperatures in the plume for L_f/H ratios less than or equal to about 2. At greater flame-height ratios, significant heat released through the ceiling itself appears to be the cause of a lack of agreement [21]. According to the L_f/H

values shown in Table 4, the Fire 4 scenario would greatly exceed the application range of Heskestad & Hamada's correlation.

4.2.1. Parameters and limitations

Eq. 3 proposed by Heskestad & Hamada [24] gives the ratio between the excess gas temperature (ΔT) at a particular radial distance r from the plume centerline and the excess gas temperature in the plume (ΔT_p) where it meets the ceiling. The equation is applied with r/b ranging from 1 to 40, where b is the effective plume radius at the intersection with the ceiling, i.e. the radius where the velocity of the impingement plume is one-half the centerline value. The expression for b is given by equation Eq. 4.

(3) $$\frac{\Delta T}{\Delta T_p} = 1.92 \cdot \left(\frac{b}{r}\right) - \exp[1.61 \cdot \left(1 - \frac{r}{b}\right)]$$

(4) $$b = 0.42 \cdot [(c_p \cdot \rho_\infty)^{4/5} \cdot T_\infty^{3/5} \cdot g^{2/5}]^{-1/2} \cdot T_p^{1/2} \cdot Q_c^{2/5} / \Delta T_p^{3/5}$$

Where c_p= 1.005 kJ·kg^{-1}·K^{-1}, ρ_∞ = 1.204 kg/m^3, T_∞ = 20 ºC , g = 9.81 m/s and Q_c (Convective Heat Release Rate in kW) and T_p (temperature at the centerline at the impingement point on the ceiling expressed in ºC) are given by Eqs. 5 and 6, respectively.

(5) $$Q_c = (1 - \chi_r) \cdot Q$$

(6) $$T_p = \Delta T_p - T_\infty$$

where Q is the Heat Release Rate in kW, ΔT_p is the excess temperature at the plume centerline at the level of the ceiling and is given by Eq. 7 [21, 27] and χ_r is assumed to be equal to 0.35, according to [28].

(7) $$\Delta T_p = 16.9 \cdot \frac{Q^{2/3}}{H^{5/3}}$$ (valid for $r/H \leq 0.18$)

It must be noted that χ_r can also be calculated using Eq. 8 proposed by McGrattan et al. [29], where $\chi_{r,max}$ =0.35, k=0.05 m^{-1} and D is the fire equivalent diameter. The application of Eq. 8 to the fire scenarios studied in this paper gives a value of χ_r =0.34, which differs from the value proposed in [28] by less than 3 %.

(8) $$\chi_r = \chi_{r,max} \cdot e^{-kD}$$

4.2.2. Application to the Valencia bridge fire tests.

Fig. 5b shows how the radial position from the centerline (r in Eq. 3) has been substituted by the longitudinal distance from the fire centerline. It should be noted that although Heskestad & Hamada's correlation [24] was defined for unconfined ceilings (i.e. where the fire is at least 3H distant from the nearest vertical obstruction [30]), it perfectly fits the experimental results for Fires 1 to 3 (where there is barely 1m between both girders). The H values were obtained by subtracting the level of the fuel at the beginning of the test (0.2 m for Fires 1, 2 and 3 and

0.8 m for Fire 4) from the level of the bottom surface of the concrete slab, which is 2.06 m. By doing so, H is 1.85 m for Fires 1 and 2, 1.55 for Fire 3 and 1.25 m for Fire 4.

Fig. 6 shows the gas temperatures throughout the Central region obtained from the Heskestad & Hamada model [24], i.e. according to Eqs. 3 to 7. Fig. 6a compares the four fire scenarios considered, whereas Fig. 6b only includes the three fire scenarios (Fires 1, 2 and 3) within the model's application range ($L_f/H \leq 2$). From these figures, it can be stated that:

- Heskestad & Hamada's model gives a good prediction of the overall shape of the temperatures along the longitudinal axis of the bridge as well as that of the peak gas temperatures. The maximum peak temperatures predicted by the model in the central region in the six sections where thermocouples where located in the experiments are 333 ºC (section S3 and S4, x=2.5 and 3.5 m) for Fire 1, 620 ºC (section S3 and S4, x=2.5 and 3.5 m) for Fire 2 and 396 ºC (section S6, x=5.5 m) for Fire 3. These values are 16.3, 18.5 and 30.4% lower than those measured in the experiment for Fires 1, 2 and 3, respectively. The differences observed can be attributed to: the existence of the girders and the abutments that confine the hotter gases, the influence of variables not included in the model (e.g. type of fuel) and to the fact that the values of some variables were taken from previous references (e.g. value of χ_r). In the particular case of Fire 3, another factor explains the temperature difference: previous research (Peris-Sayol et al. [7]) has shown that when the fire is close to the bridge abutment, the Coandă effect makes the flames adhere to the abutment walls and reach higher levels, which results in higher gas temperatures near the deck and further deck heating. This effect can be captured by advanced fire models (CFDs) but not by simplified methods such as Heskestad & Hamada's.
- The Heskestad & Hamada correlation can be used for the preliminary design of future bridge fire tests with HRR between 361 and 1130 kW. Although this model might underestimate gas temperatures up to 30.4%, it will come fairly close to the overall shape of the expected gas temperatures throughout the bridge, as well as that of the peak temperatures.
- The Heskestad & Hamada correlation cannot be used to study real bridge fires, since these events involve HRRs higher than the limit of application of the correlation (the HRR for a car is about 5 MW and for a tanker truck is about 100-200 MW according to [31, 32]). However, and since the correlation provides a good estimation of the overall shape of the temperatures along the bridge, it has the potential to be used in future, together with additional numerical and experimental work, to develop a simplified approach to study bridge fires.

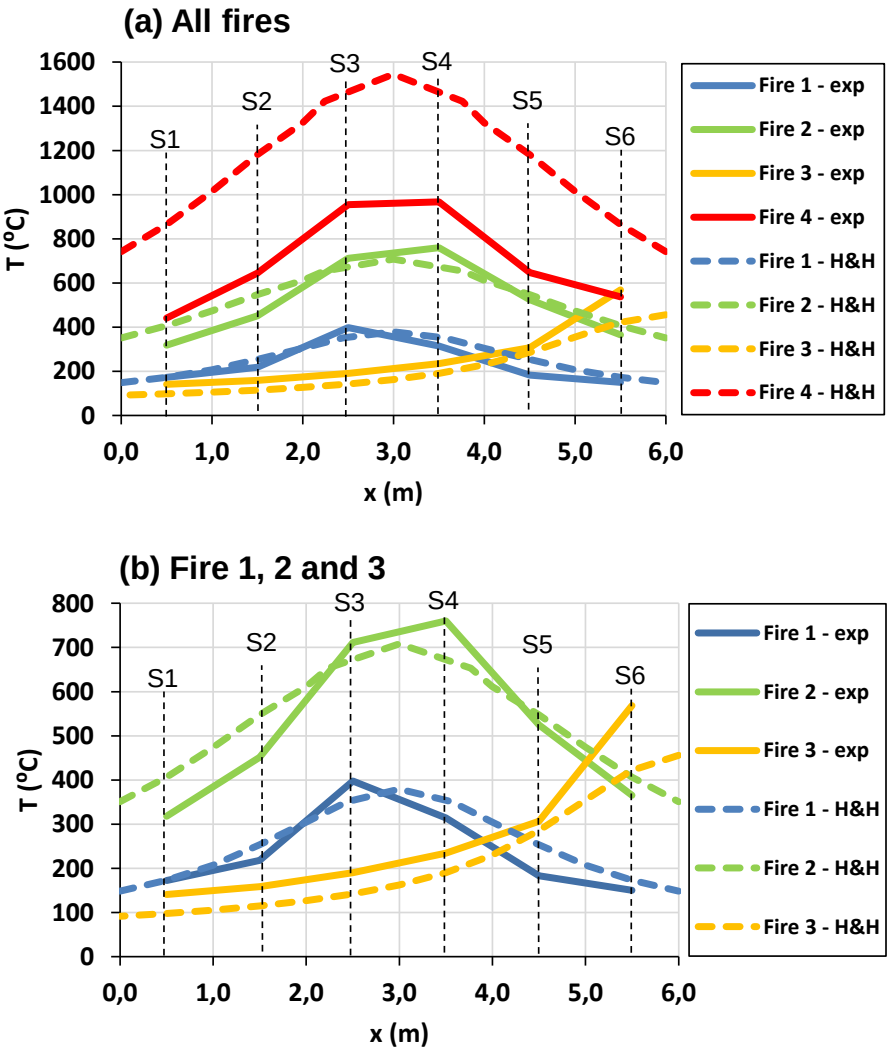

Figure 6. Central region temperatures for (a) all fire scenarios and (b) Fires 1, 2 and 3. Continuous lines are experimental values and dashed lines are those of Heskestad & Hamada's model. Experimental temperatures are the maximum recorded temperatures, not average temperatures.

Fig. 7 shows the scatter between the predicted and measured temperatures along the longitudinal axis of the bridge. The scatter in sections x=2.5 m and x=3.5 m ranges between -16 to +6 % for Fire 1 and from -12 to -18% for Fire 2. The scatter in sections x=4.5 and x=5.5 m ranges from -11 to -30% for Fire 3. These values are acceptable, considering that a scatter of 20% is considered as acceptable in much more complex models that use CFDs to solve fire engineering problems [28, 33].

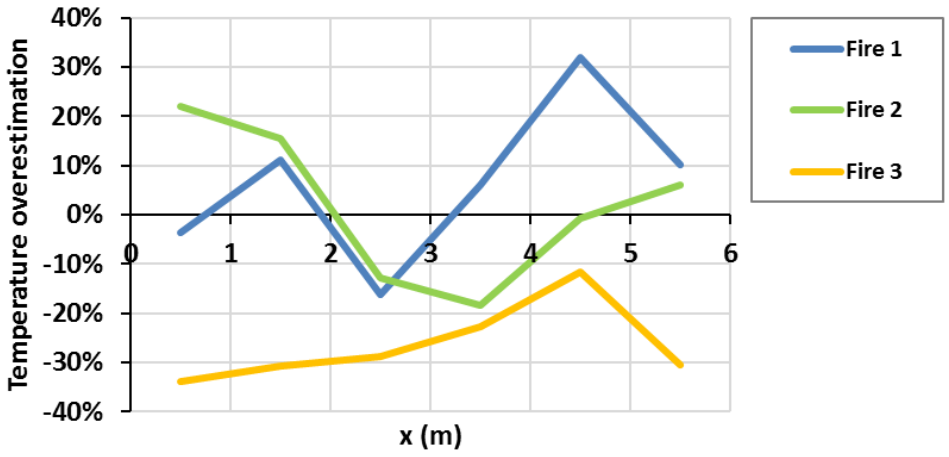

Figure 7. Scatter between the temperatures predicted in the Central region by the Heskestad & Hamada model [24] and the maximum recorded temperatures.

5. Advanced approach. Computational fluid dynamics model.

In this section, the capability of advanced calculation methods (CFD models implemented in the software Fire Dynamics Simulator) to predict the results of the Valencia bridge fire tests is studied. The Fire Dynamics Simulator (FDS) is a computational fluid dynamics (CFD) fire-driven fluid flow model [28]. The FDS hydrodynamic model solves numerically a form of the Navier-Stokes equations appropriate for low-speed (Mach number $Ma < 0.3$), thermally-driven flow, with an emphasis on smoke and heat transport in fires. The core algorithm is an explicit predictor-corrector scheme, second order accurate in space and time. Turbulence is considered by means of a Large Eddy Simulation (LES) model. The FDS uses a single step, mixing-controlled chemical reaction for the combustion model, which uses three lumped species (air, fuel and products), the last two being explicitly computed. Radiation Transport Radiative heat transfer is included in the model via the solution of the radiation transport equation for a gray gas. The equation is solved using the Finite Volume Method (FVM). The absorption coefficients of the gas-soot mixtures are computed using the RadCal narrow-band model. Although the FDS has previously been used for bridge fires (see e.g. FDS models in [4, 5, 9]), as far as the authors are aware, it has been validated for the first time in the present study for use in bridge fires by the results of a battery of bridge fire experiments. Note also that the FDS validation is valid even if the bridge dimensions and the HRR of the fire tests are smaller than those of real bridge fires because the experimental bridge and the tests were designed to reproduce the specific aspects of bridge fires.

Building an FDS model [4, 9] requires defining: (1) a control volume with its boundary conditions which represents the volume in which the entire analysis will be carried out, (2) a mesh or discretization of the control volume, (3) a geometry included in the control volume

which is submitted to fire load, (4) material properties (conductivity, density, specific heat and emissivity), (5) fire sources, (6) a combustion model, and (7) sensors or elements of the model where outputs of the analysis (e.g. temperatures) are recorded. The components of the FDS model are described below.

5.1. Control volume and mesh

The control volume used in this study is shown in Fig. 8 and includes the bridge as well as an additional volume required to properly represent the physics of the problem. It measures 12.0 m x 12.0 m x 12.0 m along the x, y and z-directions, respectively. The volume has a total of 691,000 parallelepiped cells distributed in 8 non-uniform meshes. Most of the cells have dimensions of 0.125 m x 0.125 m x 0.100 m along the *x*, *y* and *z* directions, respectively. However, *y* and *z* dimensions were reduced in some areas to 0.0625 m and 0.075 m, respectively, to obtain a finer mesh in the elements representing the deck girders and the RC slab.

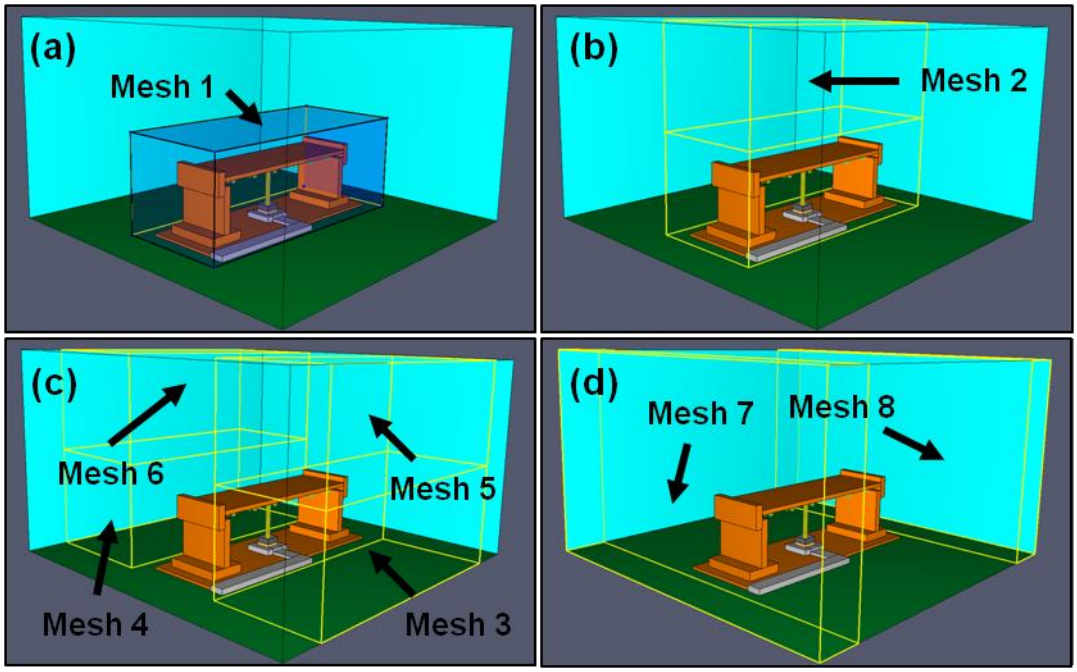

Figure 8. Eight non-uniform meshes employed for FDS model

The control volume and mesh sizes were the result of a sensitivity analysis and are a trade-off between precision and calculation times. As suggested in the FDS6 user guide [28], cell aspect ratio has been kept equal or lower than 2 in order not to penalize the efficiency of the calculation. Fig. 8 shows how the meshes were distributed along the control volume to reduce inaccuracies associated with flame and soot transfer between different meshes. Mesh 1 (see Fig. 8a) was defined to include internal flames. Similarly, soot transport was mostly limited to Meshes 1 and 2 (see Fig. 8b). Meshes 3 to 8 (see Fig. 8c and Fig. 8d) were

added to provide enough distance from the fire source to ensure that the open boundary conditions (e.g. room temperature and pressure) did not affect the results.

5.2. Geometry and materials

The bridge geometry included in the FDS model is shown in Fig. 9. It can be seen to be slightly different from the actual geometry in Fig. 1, due to the cell sizes finally employed. However, the FDS model faithfully reproduces the basic geometric parameters (vertical height 1.9 m, beam edge 0.15 m, beam centerline separation 1.0 m, and bridge width 2.0 m). Besides the geometry, each fire scenario also included an inert zone (see Fig. 10) that represented the base that supported the fuel pan and the protection of the cable to the weighing scale.

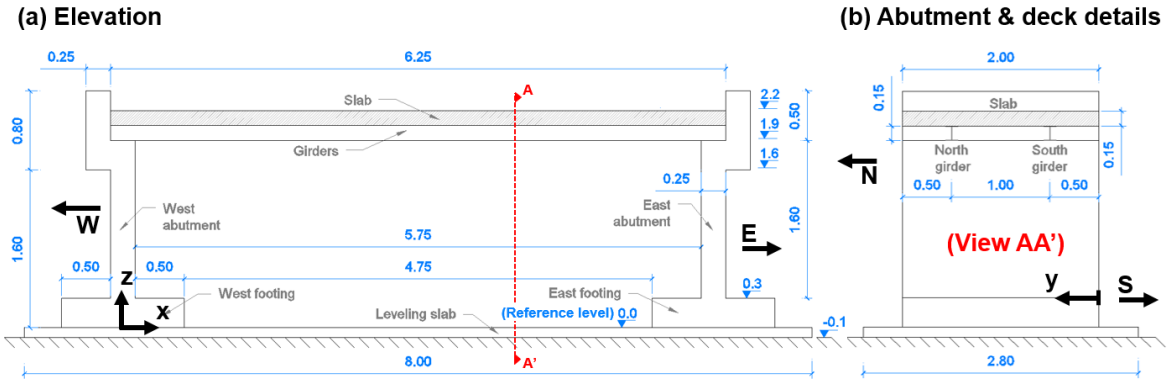

Figure 9. Bridge geometry in FDS6: (a) Elevation and (b) Abutment and deck details. All the dimensions expressed in m.

The FDS model calculates the one-dimensional heat transfer required by the definition of the thicknesses and properties of the materials used. Material thicknesses are specified in Fig. 10 and their thermal properties are given in Table 5. The FDS backing parameter (used to indicate thermal boundary conditions) was set as “Exposed” for the steel planar surfaces and “Air Gap” at room temperature for concrete obstructions.

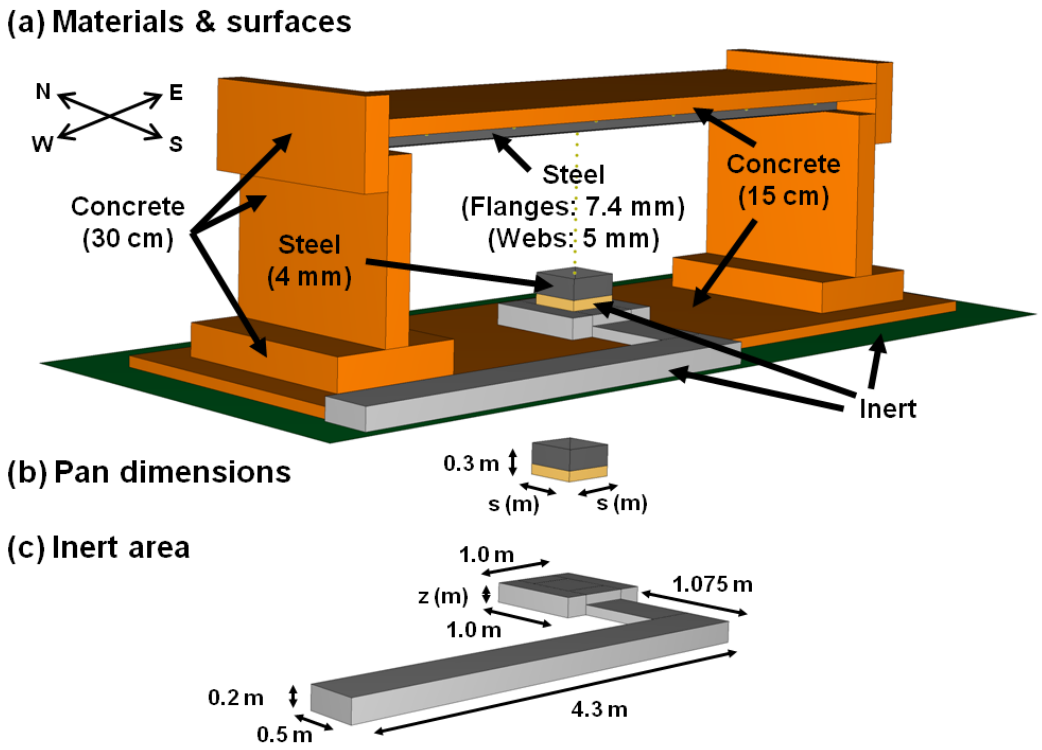

Figure 10. FDS model details: (a) Materials and surfaces, (b) Pan dimensions and (c) Inert area.

Material	Density, ρ (kg/m^3)	Specific heat, c (kJ/kg^{o}C)	Conductivity, λ (W/m^{o}C)	Emissivity, ε_m	Absorption coefficient
Steel	7850	0.46	45.8	0.95	$5{\cdot}10^4$
Concrete	2280	1.04	1.8	0.9	$5{\cdot}10^4$

Table 5. Material thermal properties. Source: Pyrosim database [34].

5.3. Fire Load and combustion model

The fire load used was defined according the weights recorded by the scale underneath the pan filled with gasoline. The FDS model was built for the four fire scenarios studied and shown in Fig. 2 and Table 4. Fig. 11 shows: (a) the HRR used as an input in the fire models, which was obtained from the mass loss rate per unit area measurements according to Eq. 9, and (b) the HRR given by the FDS software during the simulations.

(9) $$Q = A_{fire} \cdot \dot{m}'' \cdot \Delta H_c$$

Where:

Q is the heat release rate of the fire in kW

A_{fire} is the footprint of the fire in m^2. Tables 1 and 4 give side values to obtain these areas

$\dot{m}''$ is the mass loss rate per unit area in kg/m^2/s.

ΔH_c is the heat of combustion in MJ/kg. Gasoline has a 43.7 MJ/kg value [18]

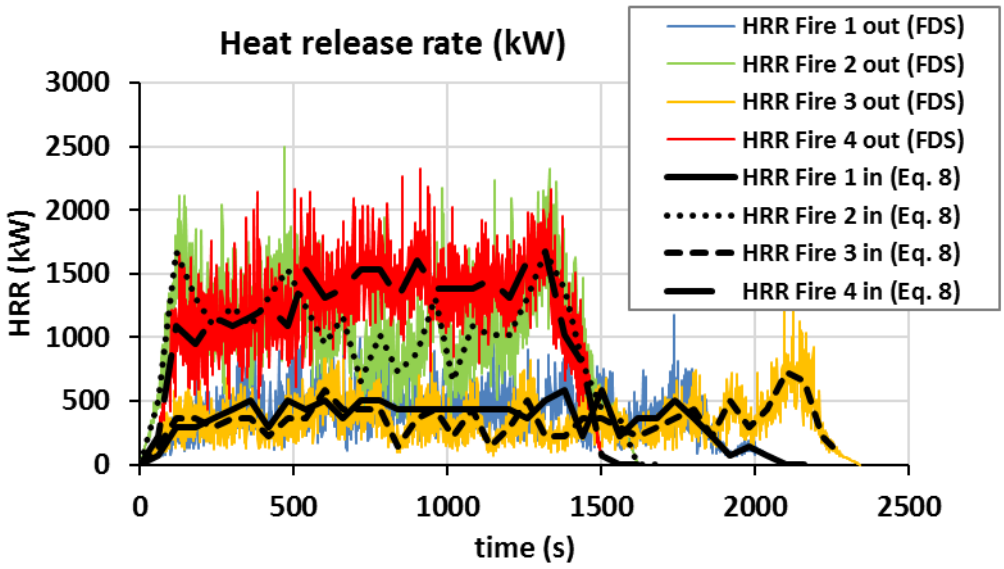

Figure 11. HRR through time for different fire scenarios: (black) defined as an FDS input and (colored) employed by FDS during the simulations.

FDS defines the fire sources through specific surfaces identified as *burners*. In the FDS simulations of the Valencia bridge fire tests, the burner that represents the fire source is a horizontal square surface of either 0.25 m^2 (Fires 1 and 3) or 0.5625 m^2 (Fires 2 and 4). The input heat curve of the release rate per unit area (HRRPUA) was defined by dividing the HRR (black curves in Fig. 11) by the corresponding burner surface. The HRR eventually used for the FDS is represented in Fig. 11 by colored lines. The average HRR and HRRPUA values for each scenario are included in Table 1 and Fig. 14, respectively. The vertical burner coordinate (z_b) for each scenario is defined in Fig. 12 and represents the level of the flames basis.

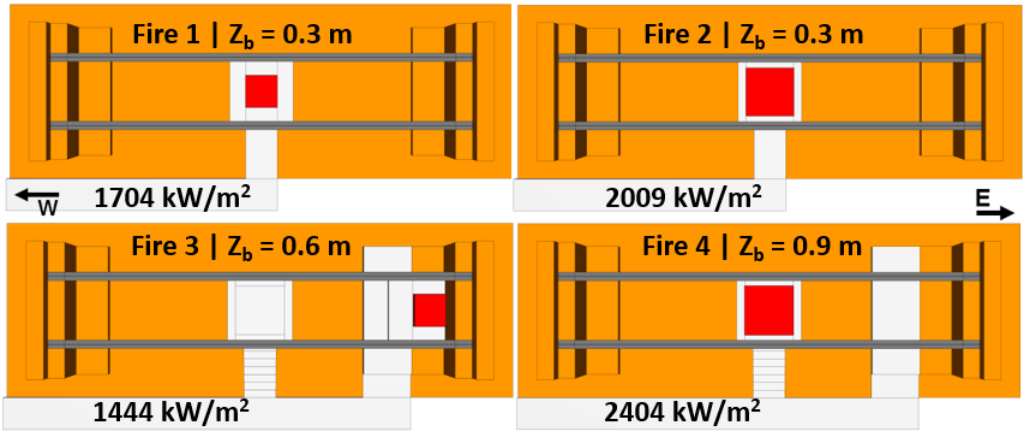

Figure 12. FDS modeling. Plan view showing the fire scenarios considered. The surface of the burner is represented in red and the steel deck beams in grey.

The fire load uses the heptane reaction provided by the Pyrosim 2016.1.0425 fuel library [34] because it is the closest to the gasoline reaction among those available. The fire load also uses the mixture fraction combustion model proposed by McGrattan et al [28, 35], with a radiation factor of 0.35. Soot yield was set to 0.037, in accordance with [36].

5.4. Sensors

The FDS model sensors are elements (usually points) that store one or more of the simulation variables and enable the output dimensions to be reduced, as they avoid the storage of variables that will not be used subsequently. Eighteen 1.5 mm diameter stainless steel sheath thermocouples were defined in the models to record temperatures that could be compared to the temperatures recorded by the real thermocouples. The FDS model includes sensors placed 5 cm below the concrete slab in six sections at x= 0.5, 1.5, 2.5, 3.5, 4.5 y 5.5 m, respectively (see Fig. 4), coinciding with the thermocouples in the horizontal TCTs (see Fig. 4). Five FDS thermocouples were also placed directly above the burner at the position of the thermocouples in the vertical TCT (see Fig. 4).

5.5. Results

Fig. 13a and Fig. 13b compare the temperatures obtained from the numerical models with those obtained experimentally. In Fig. 13a the comparison uses average temperatures during the plateau stage of the fire. In these cases, numerical models overestimate the experimental temperatures by between 30 and 120% of the experimental values (see Fig. 13c). This difference can be attributed to the wind present during the experiments, which was not allowed for in the numerical models. The wind at times blew the flames away from the vertical (see Fig. 14a), thus cooling the gases under and around the deck.

Fig. 13b compares the maximum experimental gas temperatures (which are obtained with no wind) with those predicted by the numerical models. It can be observed that the numerical models give a highly accurate prediction of both the peak values and the distribution of gas temperatures in the deck's central region. In this case, the difference between the measured and predicted temperatures (plotted in Fig. 13d) varies between -25% (Fire 2) and +30% (Fire 4). These differences are acceptable in the experimental validation of FDS models, as will be explained below (see Section 6.3.2). Figs. 14b and 14c compare Fire 4 in the experiment with the FDS's no-wind predictions and both can be seen to be remarkably similar.

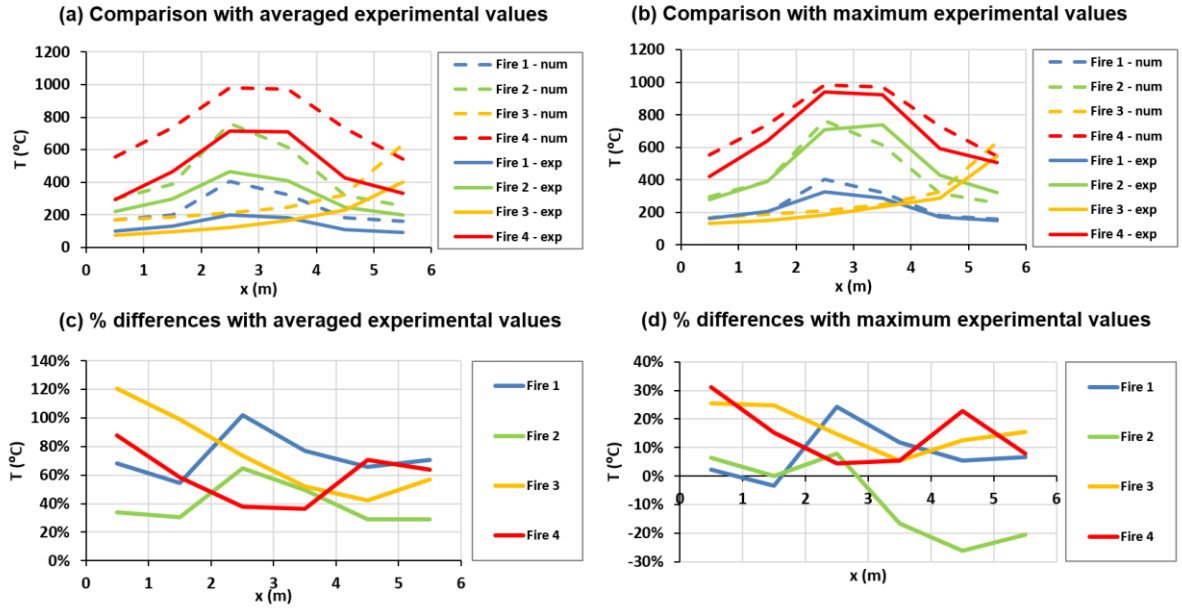

Figure 13. Comparison between experimental vs. numerical results, considering: average experimental values (a) and (c) and maximum experimental values (b) and (d). All numerical values are averages.

Fig. 15 gives the temperatures recorded in the gas through time in the section S4 (see Fig.4) in the Central and South regions for Fires 2 and 4. These scenarios were chosen because they showed the influence of the wind on the experimental temperature recordings. Similar graphs are not provided for the other tests, since the values were similar. Table 6 contains the average temperatures given by the FDS numerical models for all the fire scenarios considered. These temperatures will be compared with the temperatures recorded during the test (see Table 2) in the uncertainty analysis described in Section 6.

Figure 14. Different views of Fire 4 (a) Fire 4 test with wind (b) Fire 4 FDS model with no wind and (c) Fire 4 test with no wind.

Fig. 15a and Fig. 15b show how the experimental temperatures recorded by the GC4 thermocouple in the central region (for Fires 2 and 4 respectively) are equal to or lower than those predicted by the numerical model. Fig. 15b is especially instructive as it clearly shows that the maximum values recorded during the Fire 4 test are very similar to the values obtained with the numerical model, which can be attributed to the lesser effect of the wind during the test. On the other hand, Fig. 15c and Fig. 15d show the temperatures recorded by the GS4 thermocouple in the South region, in which the experimental temperatures are higher than the numerical temperatures, due to the wind blowing the flames towards the South and allowing the temperature to rise in this region. This confirms that average numerical temperatures and maximum experimental temperatures in the absence of wind should be used when comparing the experimental and numerical values.

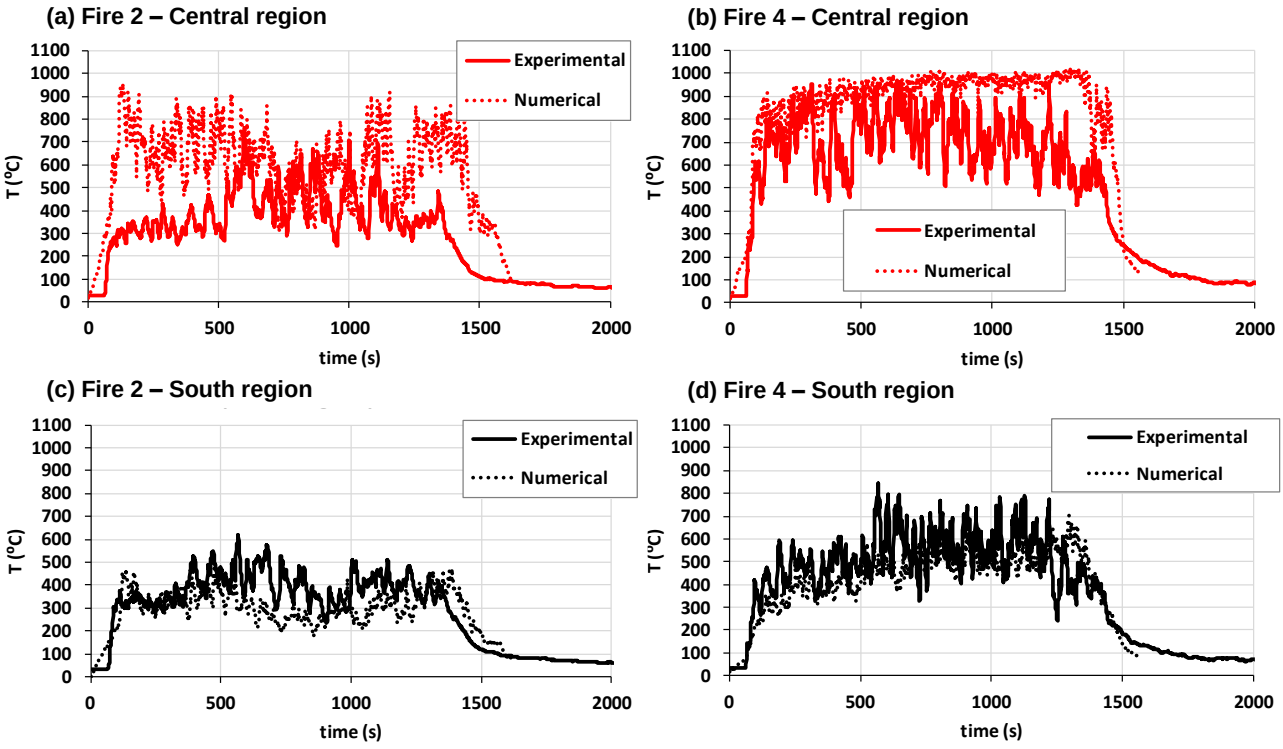

Figure 15. Time-temperature curves for the S4 deck section: (a) Fire 2 - Central region, (b) Fire 4- Central region, (c) Fire 2 - South region and (d) Fire 4 - South region. The location of the section S4 is given in Fig. 4a.

Finally, it is important to note that CFDs in general, and FDS models in particular, are complex to build and computationally expensive. For example, a typical simulation done with FDS of the fire that affected the I-65 overpass in Birmingham, Alabama, US – a bridge with a total length of 88.53 m- took three days and four hours in a computer cluster (see Alos-Moya et al. [4] for more details). Therefore, it is important to develop simplified approaches

to model the effects of fires in bridges. Such approaches could be based, for example, on improvements of existing analytical methods (such as the Heskestad and Hamada's correlation) or on the development of fire curves specific for bridges. Any of them will need validation through numerical and, if possible, experimental tests, what makes the calibration of numerical models such as the one presented in this paper of major importance.

Aver. T (ºC)	x (m)	South region	North region	Central region	z (m)	Fire plume
Fire 1	0.5	125	125	168	1.73	470
	1.5	125	125	198	1.54	520
	2.5	161	154	405	1.24	609
	3.5	150	148	322	0.99	663
	4.5	116	117	182	0.65	799
	5.5	124	123	158	-	-
Fire 2	0.5	212	210	297	1.73	768
	1.5	233	239	389	1.54	722
	2.5	342	318	762	1.24	728
	3.5	303	287	615	0.99	737
	4.5	206	203	319	0.65	746
	5.5	200	197	257	-	-
Fire 3	0.5	104	103	169	1.95	462
	1.5	82	81	191	1.69	366
	2.5	93	92	216	1.41	386
	3.5	123	121	253	1.13	487
	4.5	168	165	334	0.85	755
	5.5	241	240	643	-	-
Fire 4	0.5	361	336	554	1.89	661
	1.5	355	338	736	1.73	979
	2.5	514	443	982	1.54	983
	3.5	522	454	970	1.44	975
	4.5	367	370	729	1.25	791
	5.5	396	372	544	-	-

Table 6. Average temperatures (Ave. T (ºC)) obtained from the FDS numerical simulation. Average values were calculated during the time intervals defined in Table 3.

6. Uncertainty analysis of the results obtained using CFDs.

Differences appear when the results of a fire test are compared with those of a numerical model performed with FDS (or similar). These differences may be due to either measurement errors during the test (experimental errors, u_E) or to inaccuracies in the numerical model (model errors, u_M). The former can be attributed to incorrect measurements used as inputs in the model (e.g. mass losses and their corresponding HRR's), u_{E1}, or to incorrect experimental output measurements (e.g. gas temperatures), u_{E2}. The latter can be attributed to a number of reasons such as the differences between the real and modeled geometry, differences between the experimental HRR and the HRR finally employed (as can be seen in Fig.13) and the physical assumptions of the model (e.g. radiation factor and soot

yield parameters). Fig. 16 summarizes the sources of error mentioned above and their application to the problem studied in this paper.

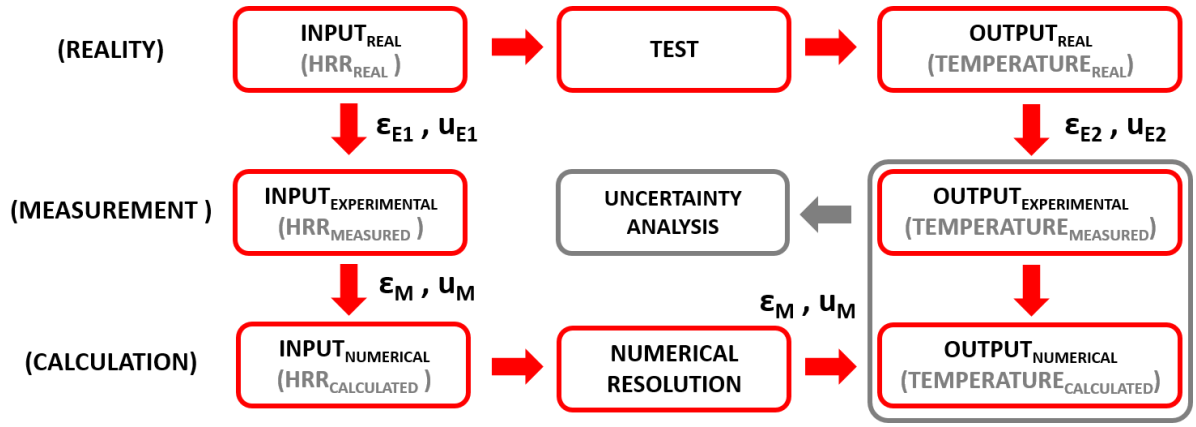

Figure 16. Sources of error and uncertainty.

In the field of fire test validation, the concept of uncertainty is more commonly used than the concept of error. Error and uncertainty express different concepts [37]: the term "error" is used: 1) to quantify the difference between the result of a measurement and the real value, or, 2) to quantify the imperfection of the method and the device used, while the uncertainty of the measurement is a non-negative parameter that characterizes the dispersion of the values attributed to a measured variable. The following subsections detail how experimental and model uncertainties are defined and how these concepts were applied to the Valencia bridge fire tests.

6.1. Experimental uncertainty

According to McGrattan [33, 38], the experimental uncertainty of a variable that a model is trying to predict is measured by *k* times the experimental relative standard deviation (ω_E) of the analyzed variable (temperature in the present study); *k* is assumed to be equal to 2 for a 95% uncertainty interval [33, 38, 39].

The experimental relative standard deviation ω_E is obtained using Eq. 10:

(10) $$\omega_E^2 = \omega_0^2 + \sum_i^n p_i^2 \cdot \omega_i^2$$

Where:

ω_o is the relative standard deviation of the output measurements and represents the uncertainty of the device which measures the quantity (temperatures in this case) that the model is trying to predict (u_{E2} defined in Fig. 16).

The expression $\sum_i^n p_i^2 \cdot \omega_i^2$ represents the u_{E2} term defined in Fig. 16. In this expression:

- p_i are factors that represent the power dependences of the individual input parameters.
- ω_i is the relative standard deviation of the input measurements and represents the uncertainty of the devices which measure the various input parameters required by the numerical model (u_{E1} defined in Fig. 16).
- *n* represents the number of relevant terms which affect the experimental uncertainty of the output variable under study. In the present study *n* is equal to 1, since the HRR is the only physical input parameter of the numerical model of the fire tests considered in the uncertainty study.

The most important physical parameters associated with the various quantities measured in the fire experiments together with their power dependence (p_i) are detailed in [39, 40].

6.2. Model uncertainty

To obtain the model uncertainty the following assumptions must be considered [39, 40]: (1) The experimental measurements are unbiased, and their uncertainty is assumed to be normally distributed with a constant experimental relative standard deviation,ω_E, and (2) the model uncertainty is normally distributed about the predicted value multiplied by a bias factor, δ. This bias factor δ indicates how, on average, the model over or under-predicts the experimental measurements [38, 39]. The model relative standard deviation of the temperature distribution is denoted as ω_M and is used to measure the scatter of the numerical output values.

Once the experimental uncertainty has been defined (by calculating the experimental relative standard deviation ω_E), and given a set of experimental measurements (E_i), as well as a corresponding set of model predictions (M_i), parameters ω_M and δ, which characterize the model uncertainty, are given by Eqs. 11 and 12, respectively [33, 38].

(11) $$\omega_M^2 + \omega_E^2 = \frac{1}{n-1} \cdot \sum_{i=1}^{n} [\ln(M_i/E_i) - \overline{\ln(M/E)}]^2$$

(12) $$\delta = \exp[\overline{\ln(M/E)} + \frac{\omega_M^2}{2} - \frac{\omega_E^2}{2}]$$

Where $\overline{\ln(M/E)}$ is given by Eq. 13

(13) $$\overline{\ln(M/E)} = \frac{1}{n} \cdot \sum_{i=1}^{n} \ln(M_i/E_i)$$

6.3. Application to Valencia bridge fire tests

6.3.1. Experimental uncertainty

In the specific case of the Valencia bridge fire tests Eq. 10 becomes Eq. 14.

(14) $\omega_E^2 = \omega_{TEMPERATURES}^2 + p_{TEMPERATURE/HRR}^2 \cdot \omega_{HRR}^2$

Where:

ω_E is the experimental relative standard deviation (σ_E / δ)

$\omega_{TEMPERATURES}$ is obtained as the combination of the uncertainties of the thermocouples and datalogger, according to Eq. 15 [41],

(15) $\omega_{TEMPERATURES}^2 = \omega_{THERMOCOUPLES}^2 + \omega_{DATALOGGER}^2$

$p_{TEMPERATURE/HRR}^2$ is equal to 2/3 according to [39, 40]. This factor provides the temperature uncertainty directly attributable to the uncertainty of the HRR measurements.

ω_{HRR} is the uncertainty associated with HRR measurement.

Using the values $\omega_{THERMOCOUPLES} = 0.75\%$, $\omega_{DATALOGGER} = 0.25\%$ y $\omega_{HRR} = 15.00\%$ provided by the manufacturers of the devices and by [40], the experimental relative standard deviation, ω_E, is 10.03%. Thus, adopting a factor *k* equal to 2, as explained in Section 6.1 for a 95% uncertainty interval, the experimental relative uncertainty is 20.06%.

6.3.2. Model uncertainty

As explained in Section 6.2, the model uncertainty requires the calculation of ω_M and δ from the experimental temperature values (E_i) and from the temperatures obtained by the numerical models (M_i).

Fig. 17 gives the dispersion between the maximum experimental temperatures and the average temperatures obtained from the numerical models for the four fire scenarios. Fig. 17a includes the values recorded by the thermocouples in the ceiling jet zone (horizontal thermocouple trees in the three regions (South, Central and North) of the bridge deck). It can be seen that the numerical model's values show a bias factor (δ) of 1.0982 with respect to the experimental values. This dispersion of the results is due to the assumptions of the FDS model, the uncertainties in the input parameters of the FDS model (e.g. soot yield and radiation fraction) and the effect of the wind. The latter variable, even though in theory belonging to the experimental uncertainty, could not be separated from the numerical uncertainty, simply because both its magnitude and direction keep changing with time. This phenomenon will be repeated in any future tests carried out under windy conditions. Fig. 17b gives similar data for the vertical thermocouple tree in the fire plume. In this case fewer data are used than for the ceiling jet (20 instead of 70).

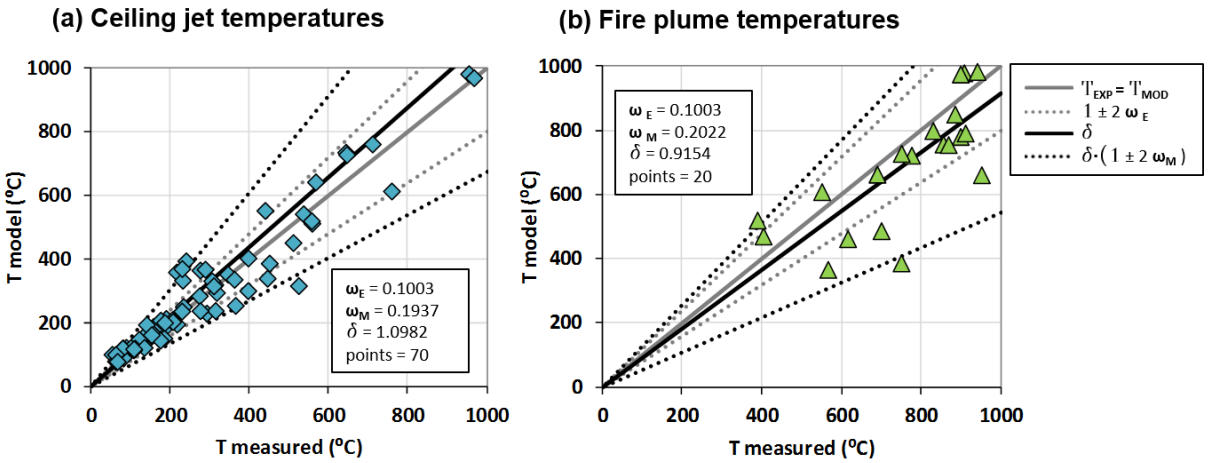

Figure 17. Scatter between measured and model temperatures for: (a) Ceiling jet and (b) Fire plume

Tables 7 and 8 compare the parameters used to measure the uncertainty (without and with the wind correction given in Section 5.5) with those obtained by McGrattan et al. [33] in the FDS validation tests. It should be noted that both the bias factor and the relative standard deviation of the models are closer to the parameters of McGrattan et al. [33] when maximum experimental temperatures where used. The higher uncertainties obtained in the present study can be explained by the influence of wind, a variable absent in the FDS validation work presented in [33]. Given these considerations, the authors consider the validation of the FDS model carried out is correct.

Ceiling jet	ω_E	ω_M	δ	Points
Valencia bridge fire tests (Averaged temperatures)	0.1	0.237	1.291	70
Valencia bridge fire tests (Maximum temperatures)	0.1	0.194	1.098	70
McGrattan et al. [33]	0.07	0.14	1.05	898

Table 7: Uncertainty parameters for ceiling jets. 70 measurements considered.

Fire plume	ω_E	ω_M	δ	Points
Valencia bridge fire tests (Averaged temperatures)	0.1	0.346	1.518	20
Valencia bridge fire tests (Maximum temperatures)	0.1	0.202	0.915	20
McGrattan et al. [33]	0.07	0.16	1.18	107

Table 8: Uncertainty parameters for fire plumes. 20 measurements considered.

7. Conclusions and future work

This paper compares the experimental gas temperatures recorded in tests 2, 4, 7 and 8 of the Valencia bridge fire tests [17] with the temperatures predicted by both a simplified correlation and a computational fluid dynamics model. The comparison between the experimental data and the advanced numerical approach was conducted in two steps. Firstly, a more visual comparison was included in order to determine where the higher differences were taking place. An uncertainty analysis was then carried out to compare model uncertainties with other similar tests validated in the FDS validation guide [33]. From these analyses, the following conclusions can be drawn:

- Since the tests were carried out in the open air, they were significantly affected by the wind, unlike tests performed in furnaces or closed spaces. The wind blew the flames away from the vertical plane and also affected the ascending column of gases from the fuel pan under the deck.
- The four fire scenarios were validated with a slightly higher uncertainty than that obtained by McGrattan et al. [33]. The higher numerical dispersion can be attributed mainly to the effect of the wind during the tests carried out in the present study. In order to reduce the uncertainty values, it is recommended that a wind break should be used in any future studies of this type.
- Both the simplified and the advanced approaches provide good results when used to predict gas temperatures for the Fires 1, 2 and 3 scenarios if the zero wind velocity correction justified in Section 5.5 is applied. Temperatures in the Fire 4 scenario can be accurately predicted by the FDS model, but not by the Heskestad & Hamada correlation, as the HRR in this scenario is higher than the correlation application limits.
- Although Heskestad & Hamada's model was initially defined for unconfined fires, it can be used for the preliminary design of future bridge fire tests with HRRs between 361 and 1130 kW. Although gas temperatures may be underestimated by up to 30.4%, it will give a good approximation of the overall shape of both peak temperatures and the expected gas temperatures around the bridge.
- The Heskestad & Hamada correlation cannot be used to study real bridge fires as it was developed for fires with a maximum HRR of 764 kW, which is much lower than the HRR of the fire loads involved in real bridge fires. However, given its good prediction of the overall shape of gas temperatures, it has the potential to be used as the starting point for a new simplified approach to predict gas temperatures in bridge fires.

This research work has validated the application of CFD models built with the software FDS for the study of bridge fires and has corroborated the application limits of a common simplified approach for ceiling jets. It is therefore an important step forward in the study of the effects of fires in bridges and improving the resilience of infrastructure networks vis-à-vis fire hazards. It has also highlighted the problems that could arise in fire tests in the open air, especially the influence of the wind. Future experimental work in this area should first consider ways of reducing wind to avoid a source of uncertainty. Then specific tests should be designed and carried out under wind controlled conditions to study wind influence. Future numerical work can be addressed towards the development of simplified approaches to model bridge fires based e.g. on improvements of existing analytical methods (such as the Heskestad and Hamada's correlation) or on the development of fire curves specific for bridges. Any of these simplified approaches will need validation through numerical and, if possible, experimental tests, what makes the work presented in this paper of major importance.

8. Acknowledgements

Funding for this research was provided by the Spanish Ministry of Science and Innovation (Research Project BIA 2011–27104). The authors are grateful to the Infrastructure and Safety departments of the Universitat Politècnica de València and the City of Valencia Fire Department (*Cuerpo de Bomberos de Valencia*), which provided crucial support in conducting the tests.

References

[1] Peris-Sayol G, Paya-Zaforteza I, Balasch-Parisi S, Alos-Moya J. Detailed Analysis of the Causes of Bridge fires and Their Associated Damage Levels. ASCE Journal of Performance and Constructed Facilities. 2016. doi:10.1061/(ASCE)CF.1943-5509.0000977

[2] Garlock ME, Paya-Zaforteza I, Gu L, Kodur V. Fire hazard in bridges: review, assessment and repair strategies. Engineering Structures 2012; 35:89-98.

[3] Quiel SE, Yokoyama T, Bregman LS, Mueller KA, Marjanishvili SM. A streamlined framework for calculating the response of steel-supported bridges to open-air tanker truck fires. Fire Safety Journal 2015; 73:63-65.

[4] Alos-Moya J, Paya-Zaforteza I, Garlock MEM, Loma-Ossorio E, Schiffner D, Hospitaler A. Analysis of a bridge failure due to fire using computational fluid dynamics and finite element models. Engineering Structures 2014; 68:96-110.

[5] Gong X, Agrawal AK. Numerical Simulation of Fire Damage to a Long-Span Truss Bridge.Journal Bridge Engineering 2015;20(10). doi: 10.1061/(ASCE)BE.1943-5592.0000707#sthash.nhj5KqVo.dpuf

[6] Godart B, Berthellemy J, Lucas JP. Diagnosis, assessment and repair of the Mathilde bridge close to collapse during a fire. Structural Engineering International. 2015;25(3):331-38.

[7] Peris-Sayol G, Alos-Moya J, Paya-Zaforteza I, Hospitaler-Perez A. A parametric study on the thermo-mechanical response of a multi-girder steel bridge submitted to real fires.Informes de la Construcción, 66 (Extra-1) (In Spanish).

[8] Nahid MNH, Sotelino ED, Lattimer BY. Thermo-Structural Response of Highway Bridge Structures with Tub Girders and Plate Girders. Journal of Bridge Engineering 2017, 22 (10).

[9] Peris-Sayol G, Paya-Zaforteza I, Alos-Moya J, Hospitaler A. Analysis of the influence of geometric, modeling and environmental parameters on the fire response of steel bridges subjected to realistic fire scenarios. Computers and Structures 2015; 158:333-345.

[10] Paya-Zaforteza I, Garlock M. A numerical investigation on the fire response of a steel girder bridge. Journal of Constructional Steel Research 2012; 75: 93-103.

[11] Buchanan AH. Structural Design for Fire Safety.John Wiley & Sons, Chichester, United Kingdom, 2002.

[12] Albero V, Saura H, Hospitaler A, Montalvà JM, Romero ML. Optimal design of prestressed concrete hollow core slabs taking into account its fire resistance. Advances in Engineering Software 2018 122: 81-92.

[13] Quiel SE, Garlock MEM, Paya-Zaforteza I. Closed Form Procedure for Predicting the Capacity and Demand of Steel Beam-Columns under Fire. ASCE Journal of Structural Engineering 2011; 137: 967-76.

[14] Rackauskaite E., Kotsovinos, P, Jeffers A., Rein G. Structural analysis of multi-storey steel frames exposed to travelling fires and traditional design fires. Engineering Structures 2017 150: 271-287.

[15] Maraveas C, Vrakas A. Design of concrete tunnel linings for fire safety. Structural Engineering International 2014 24 (3): 319-329.

[16] Ji J, Tong Q, Wang L, Lin C, Zhang C, Gao Z, Fang J. Application of the EnKF method for real-time forecasting of smoke movement during tunnel fires. Advances in Engineering Software 2018 115: 398-412.

[17] Alos-Moya J, Paya-Zaforteza I, Hospitaler A. Valencia bridge fire tests: Experimental study of a composite bridge under fire. Journal of Constructional Steel Research 2017 138: 538-554.

[18] Babrauskas V. Chapter 26. Heat Release rates. In: SFPE handbook of fire protection engineering, 5th ed. 2016. p. 799-904.
[19] Peris-Sayol G, Paya-Zaforteza I, Balasch-Parisi S., Alos-Moya J. Analysis of the Factors that Influence the Maximum Adiabatic Temperatures in I-girder Bridges. 9th International Conference on Structures in Fire, p. 743-50, Princeton, NJ, USA; 2016
[20] Quiel S, Zhu Z, Mueller K, Carlton A, Marjanishvili S. Performance-Based Prioritization of Fire Mitigation for Highway Bridges. 9th International Conference on Structures in Fire, p. 776-83, Princeton, NJ, USA; 2016
[21] Alpert RL. Chapter 14. Ceiling jet flows. In: SFPE handbook of fire protection engineering, 5th ed. 2016. p. 429-54.
[22] Hasemi Y, Yokobayashi S., Wakamatsu T, Ptchelintsev A. Fire Safety of Building Components Exposed to a Localized Fire: Scope and Experiments on Ceiling/Beam System Exposed to a Localized Fire. AsiaFlam 95 - 1st International Conference, p. 351, London, UK; 1995
[23] Alpert RL. Turbulent ceiling jet induced by large scale fires. Combustion Science and Technology 1975; 11:197-213.
[24] Heskestad G, Hamada T. Ceiling Jets of Strong Fire Plumes. Fire Safety Journal 1993; 21:69-82
[25] Heskestad G. Chapter 13. Fire plumes, flame height, and air entrainment. In: SFPE handbook of fire protection engineering, 5th ed. 2016. p. 396-428.
[26] KoslowskiCC and Motevalli V.Behavior of a2-Dimensional Ceiling Jet Flow: A Beamed Ceiling Configuration. Fire Safety Science - Proceedings ofthe Fourth International Symposium, p. 469, Bethesda, MD; USA;1994.
[27] Alpert RL. Calculation of Response Time of Ceiling-Mounted Fire Detectors. Fire Technology,1972:8:181. doi:10.1007/BF02590543
[28] McGrattan K, Hostikka S, McDermott R, Floyd J, Weinschenk C, Overholt K. Fire Dynamics Simulator User's Guide (version 6). User's Guide.NIST Special Publication 1019, Gaithersburg, MD, USA; 2013.
[29] McGrattan K.B., Baum H.R., Hamins A. Thermal radiation from Large Pool Fires. NIST Report NISTIR 6546, 2000.
[30] Drysdale D. An Introduction to Fire Dynamics.John Wiley and Sons. United Kingdom; 2011
[31] Cheong MK, Spearpoint M J, Fleischmann CM. Design fires for vehicles in road tunnels. 7th International Conference on Performance-Based Codes and Fire Safety Design Methods, Auckland, New Zealand; 2008; 229-240

[32] Ingason H. Design fires in tunnels. 2nd International Symposium. Safe & Reliable Tunnels Inovative European Achievements, Lausanne; 2006
[33] McGrattan K, Hostikka S, McDermott R, Floyd J, Weinschenk C, Overholt K. Fire Dynamics Simulator Technical Reference Guide. Volume 3: Validation (version 6). NIST Special Publication 1018-3, Gaithersburg, MD, USA; 2013.
[34] Thunderhead Engineering. Pyrosim User Manual. Included in Pyrosim version 2016.1.0425.
[35] McGrattan K, Hostikka S, McDermott R, Floyd J, Weinschenk C, Overholt K. Fire Dynamics Simulator Technical Reference Guide. Volume 1: Mathematical Model (version 6). NIST Special Publication 1018, Gaithersburg, MD, USA; 2013.
[36] Hurley MJ. Appendix 3: Fuel Properties and Combustion Data. In: SFPE handbook of fire protection engineering, 5th ed. 2016. p. 3437-3475.
[37] Centro español de la metrología. Evaluación de datos de medición. Guía para la expresión de la incertidumbre de medida. 2008
[38] McGrattan K, Steward Miles S. Chapter 32. Modeling Fires Using Computational Fluid Dynamics (CFD). In: SFPE handbook of fire protection engineering, 5th ed. 2016. p. 1034-1065.
[39] McGrattan K, Toman B. Quantifying the predictive uncertainty of complex numerical models. Metrologia. 2011; 48:173-80
[40] Hamins A. Verification and Validation of Selected Fire Models for Nuclear Power Plant. Applications. Volume 7: Experimental Uncertainty. U.S. Nuclear Regulatory Commission, Office of Nuclear Regulatory Research (RES), Rockville, MD, and Electric Power Research Institute (EPRI), NUREG-1824 and EPRI 1011999, Palo Alto, CA USA; 2006.
[41] Gutierrez-Montes C, Sanmiguel-Rojas E, Kaiser AS, Viedma A. Numerical model and validation of atrium enclosure fire in a new fire test facility. Building and Environment 2008; 43:1912-1928.
[42] Rivkin CH. Section 21: Transportation Fire Safety. In: Fire Protection Handbook. NFPA 502, Standard for Road Tunnels, Bridges and Other Limited Access Highways, 2008. p. 502-23.